Photophysics of the π,π^* and n,π^* States of Thymine: MS-CASPT2 Minimum-Energy Paths and CASSCF on-the-Fly Dynamics

David Asturiol,[†] Benjamin Lasorne,[‡,§] Michael A. Robb,[§] and Lluís Blancafort*[,⊥]

Institut de Química Computacional, Parc Científic i Tecnològic de la Universitat de Girona, Edifici Jaume Casademont, Pic de Peguera 15 (la Creueta), 17003 Girona, Spain, CTMM, Institut Charles Gerhardt, UMR 5253, CC 1501, Université Montpellier II, 34095 Montpellier Cedex 5, France, Department of Chemistry, Imperial College London, London SW7 2AZ, U.K., and Institut de Química Computacional, Departament de Química, Universitat de Girona, Campus Montilivi, 17071 Girona, Spain

Received: June 5, 2009; Revised Manuscript Received: July 23, 2009

The photodynamics along the main decay paths of thymine after excitation to the lowest π,π^* state have been studied with MS-CASPT2 calculations and semiclassical CASSCF dynamics calculations including a surface hopping algorithm. The static calculations show that there are two decay paths from the Franck−Condon structure that lead to a conical intersection with the ground state. The first path goes directly to the intersection, while the second one is indirect and involves a minimum of the π,π^* state, a small barrier, and a crossing between the π,π^* and n,π^* states. From the static calculations, both paths have similar slopes. The dynamics calculations along the indirect path show that, after the barrier, part of the trajectories are funneled to the intersection with the ground state, where they are efficiently quenched to the ground state. The remaining trajectories populate the n,π^* state. They are also quenched to the ground state in less than 1 ps, but the static calculations show that the decay rate of the n,π^* state is largely overestimated at the CASSCF level used for the dynamics. Overall, these results suggest that both direct and indirect paths contribute to the subpicosecond decay components found experimentally. The indirect path also provides a way for fast population of the n,π^* state, which will account for the experimental picosecond decay component.

Introduction

Pump−probe spectroscopy experiments with femtosecond resolution have provided evidence for ultrafast, radiationless relaxation mechanisms of the DNA and RNA nucleobases after photon absorption.[1−9] While this is usually interpreted as a mechanism of self-protection of DNA toward UV radiation, it is also known that exposure of DNA-like oligomers and DNA itself to UV induces formation of potentially mutagenic cyclobutane pyrimidine dimers.[10] Significant experimental and theoretical efforts have been carried out in the past decade to clarify this complex picture, and the calculations aim to provide the mechanistic explanation for the lifetimes and multiexponential decay components found for the nucleobases in the gas phase, in water, and in the DNA environment.[11] In this context, the aim of this paper is to study the photodynamics of isolated thymine after excitation to the lowest π,π^* state and clarify some mechanistic aspects of the decay. We have approached this problem combining static and dynamics studies of the potential energy surface. In principle, the dynamics allow for a simulation of the decay time scale and the branching of trajectories when conical intersections are involved, but because of their high computational cost, they must be carried out at lower levels of theory than the static studies. This practical restriction can affect the validity of the dynamics results since they are very sensitive to the level of theory. Therefore, the interpretation of the dynamics is completed with a critical evaluation by comparison with the higher-level static calculations.

Experimentally, the photodynamics of thymine in the gas phase have been described in terms of relaxation components on the subpicosecond, picosecond, and nanosecond range. The first pumb−probe transient experiments in the gas phase reported a biexponential decay with components of 6.4 and 100 ps, respectively.[3,12] However, a three step decay mechanism with components of <50 fs, 490 fs, and 6.4 ps was described later on by Ullrich et al.[7] More recently, in a study with 80 fs resolution, Canuel et al.[1] reported a biexponential decay with components of 105 fs and 5.12 ps, respectively. The origin of the subpicosecond deactivation components is usually assigned to barrierless relaxation from the bright π,π^* state to the ground state (GS), but the origins of longer components are subject to discussion. Thus, the ps transient has been assigned to deactivation from the optically dark n,π^* state[8,9] and to a close-lying triplet state, $^3\pi,\pi^*$.[3,12] In addition to that, a long-living dark state (hundreds of ns) has also been proposed[8,9] to arise from the n,π^* state.

On the theoretical side, several studies have highlighted the role of a conical intersection between the first excited and the ground state in the ultrafast decay, both for thymine and uracil. The intersection structure, $\mathbf{(Eth)_X}$, is of ethylene type and is characterized by an out-of-plane bending of the C_5 substituent (a hydrogen atom in uracil and a methyl group in thymine; see Figure 1 for the numbering). It has been located at several levels of theory,[13−20] and the mechanisms proposed to explain the experimental decay vary depending on the level of theory. In short, two paths to access the intersection have been described with complete active space self-consistent field (CASSCF) and complete active space second-order perturbation (CASPT2)

* To whom correspondence should be addressed. E-mail: lluis.blancafort@udg.edu.
[†] Parc Científic i Tecnològic de la Universitat de Girona.
[‡] Université Montpellier II.
[§] Imperial College London.
[⊥] Universitat de Girona.

10.1021/jp905303g CCC: $40.75
Published on Web 09/01/2009

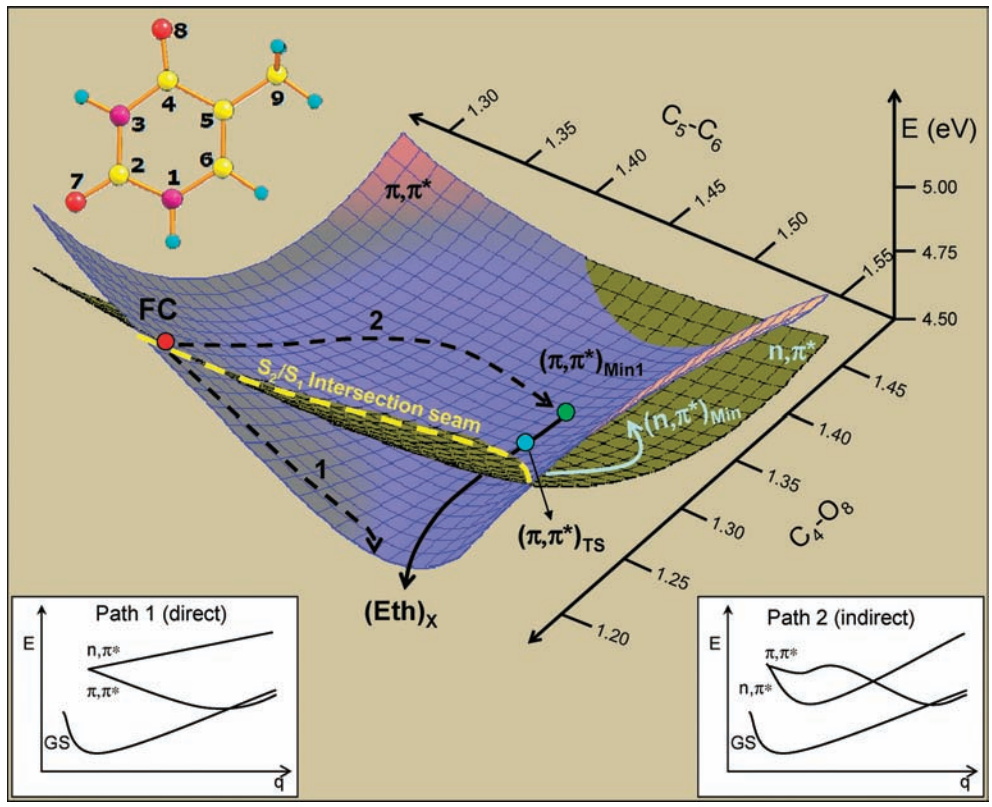

Figure 1. Two-dimensional sketch of the two lowest excited-state potential energy surfaces (S_1 and S_2) of thymine in the vicinity of the Franck−Condon region. Insets: FC structure with atom numbering and energy profiles for the paths contained in the two-dimensional sketch.

calculations. The corresponding one-dimensional energy profiles are shown as insets in Figure 1, together with a two-dimensional sketch of the potential energy surface in the vicinity of the Franck−Condon region, which shows the two paths (see also Figure 8 of ref 13). Path 1 is a barrierless, direct path from the Franck−Condon (FC) structure to $\mathbf{(Eth)_X}$ on the lowest-lying, spectroscopically active π,π^* state.[16] In the mechanism based on path 1, the subpicosecond decay component reflects the decay to the ground state, and the picosecond component is proposed to arise from consumption of a planar minimum of the π,π^* state and/or a nonplanar minimum of the n,π^* state, which are also populated during the decay.[16,18] In contrast to this, path 2 is indirect and goes through a nonplanar minimum of the π,π^* state, namely, $\mathbf{(\pi,\pi^*)_{Min}}$. This minimum is separated from $\mathbf{(Eth)_X}$ by a barrier and a crossing with the n,π^* state. Multiple-spawning dynamics trajectories run at the CASSCF level[13] follow the indirect path and remain trapped at $\mathbf{(\pi,\pi^*)_{Min}}$ before accessing the intersection with the ground state. On the basis of these results, it has been suggested that the subpicosecond component (<50 fs) corresponds to decay from the FC structure to $\mathbf{(\pi,\pi^*)_{Min}}$, while the picosecond component reflects the depopulation of the $\mathbf{(\pi,\pi^*)_{Min}}$ intermediate. A third explanation has been proposed on the basis of semiempirical OM2//MRCI dynamics[14] with a trajectory surface hopping algorithm. In this case, two different relaxation mechanisms are observed in the subpicosecond range. The fastest mechanism corresponds to direct decay from the FC structure to $\mathbf{(Eth)_X}$ and explains the <50 fs component, while the other mechanism is assigned to the 490 fs component and corresponds to decay from the π,π^* state to the n,π^* state and further to the ground state. Finally, nonadiabatic molecular dynamics[21] for uracil using density functional theory give a lifetime of approximately 600 fs for the π,π^* state, which decays through the ethylenic intersection. However, the n,π^* state was not considered in these calculations.

In view of the discrepancies between these theoretical results, the objective of the present paper is to gain further insight into the relaxation process of thymine. For this purpose, we have recalculated the direct and indirect paths in a uniform manner, using the MS-CASPT2//CASSCF approach (MS-CASPT2 calculations along the optimized CASSCF paths), which is one of the approaches of reference for accurate excited-state calculations. Moreover, we have carried out semiclassical, on-the-fly, dynamics calculations along the indirect path. In the dynamics calculations, the nuclei are propagated classically on a CASSCF potential energy surface, and the passage through the conical intersections is treated with a trajectory surface hopping algorithm (see Computational Details). This methodology has been applied before to several photochemical and photophysical problems,[22−25] and a similar implementation at the multireference configuration interaction (MR-CI) level has been applied to study the decay of adenine.[26] The starting scenario for our dynamics is the two-dimensional surface of Figure 1. Similar models have been previously proposed in refs 13 and 16. For simplicity, the surface is sketched along the C_4-O_8 and C_5-C_6 stretching coordinates, although the actual paths are more complicated and involve other coordinates that correspond to out-of-plane modes, such as C_6 pyramidalization and C_5-C_6 bond torsion. The two paths coexist on the surface and merge as they approach $\mathbf{(Eth)_X}$. The CASSCF trajectories started at the FC structure in ref 13 follow the indirect path and get trapped in $\mathbf{(\pi,\pi^*)_{Min}}$ for a time that exceeds the time range of our studies, which is of a few hundreds of femtoseconds. Therefore, we have studied the second step of this path (full line in Figure 1), starting our trajectories from the transition state $\mathbf{(\pi,\pi^*)_{TS}}$ that separates this minimum from $\mathbf{(Eth)_X}$. Because of the limitations of the CASSCF level of theory used for the dynamics, the information that we can obtain from the trajectories is mainly mechanistic. For this reason, and due to the computational cost of the

trajectories, we have run a reduced number of trajectories, where we have sampled the main paths encountered after $(\pi,\pi^*)_{TS}$ with 14 trajectories. This combined static and dynamics approach shows that both paths provide a rapid deactivation route to the ground state through the ethylenic intersection, $(Eth)_X$, while the indirect path is also a route to populate the n,π^* state, where the system can get trapped for a longer time.

Computational Details

MS-CASPT2//CASSCF Potential Energy Surface. The static calculations were carried out at the MS-CASPT2//CASSCF level of theory, using the 6-311G* basis set. Optimizations and minimum-energy-path calculations have been performed at the CASSCF level using Gaussian03,[27] with no symmetry restrictions. The minimum-energy paths were obtained with the intrinsic reaction coordinate[28] and initial relaxation decay techniques[29] in mass-weighted Cartesian coordinates. The displacements are given in bohr times the square root of the atomic mass unit (atomic units, au).

A (12,9) active space consisting of the eight π orbitals and the O_8 lone pair was used for the optimization of structures $(\pi,\pi^*)_{Min}$, $(n,\pi^*)_{Min}$, $(n,\pi^*/GS)_X$, and $(n,\pi^*/\pi,\pi^*)_X$ and the intrinsic reaction coordinate calculations involving these structures. Equal state average over the two higher states has been used in the optimizations whenever possible. In the cases with three states where convergence could not be achieved, the three states were averaged with equal weights. In the state-averaged optimizations using nine active orbitals, solution of the state-averaged coupled perturbed multiconfigurational SCF (SA-CPMCSCF) equations was not feasible, and the orbital rotation contributions to the gradients were neglected.[30] Structure $(Eth)_X$ and the minimum-energy path from the FC point to that structure were optimized with a smaller (10,8) active space, where the oxygen lone pair was removed because its occupation was close to 2.0. Structure $(\pi,\pi^*)_{TS}$ was also optimized with a (10,8) active space to solve the SA-CPMCSCF equations and calculate the orbital rotation contributions to the gradient, thus allowing for an analytical frequency calculation. In this case, the π orbital with highest occupation was removed from the active space. The minimum-energy-path calculations from this transition structure were also carried out with the (10,8) active space.

MS-CASPT2 single-point calculations have been carried out with Molcas5.4.[31] All energies in eV discussed in the paper are relative to the MS-CASPT2 ground-state energy (CASSCF(10,8)/6-311G* optimized geometry). The MS-CASPT2 calculations were carried out with a CASSCF(12,9)/6-311G* reference wave function over the six lowest roots because close-lying higher states in some regions of the potential energy surface make the inclusion of six roots necessary to obtain smooth profiles for the lowest π,π^* and n,π^* states. In all cases, state-averaging over all states with equal weights and a real level shift[32] parameter of 0.3 were used.

For a better comparison between the MS-CASPT2 static calculations and the CASSCF dynamics, the critical points were reoptimized at the CASSCF(8,6)/6-31G* level (see below for the active space orbitals). In this case, the connection between the critical points at the CASSCF level was confirmed by linear interpolations in internal coordinates between the structures (see Figure 3 for the single-point energies and SI1, Supporting Information, for the complete energy profiles).

CASSCF Semiclassical Dynamics. We have carried out semiclassical direct dynamics trajectories,[33−35] where the nuclear gradient and Hessian are calculated "on-the-fly" in the full space of $3N - 6$ coordinates (where N is the number of atoms) and the nuclei are propagated classically. The calculations have been carried out with a development version of Gaussian03[36] at the CASSCF(8,6)/6-31G* level. The trajectories where started on S_2, and when they approached a region of S_2/S_1 degeneracy (threshold of 8 mhartrees), the CASSCF surface hopping algorithm was activated. In this algorithm, the time-dependent electronic wave function is calculated and the surface hopping probabilities are obtained by projecting the time-dependent wave function on the CASSCF states. Hops occur when the probabilities for the running state go below a threshold of 0.20 (see the Supporting Information of ref 37 for more details). The current implementation of this algorithm only allows for state-averaging between the two highest excited states. For this reason, after the hops from S_2 to S_1, the trajectories were stopped once the S_2-S_1 energy gap went over a threshold of 10 mhartree, and they were restarted on S_1 using the final geometry and velocity of the first run.

The length of the trajectories (approximately 500 fs, with approximately 2 steps per fs) and the need to calculate accurate gradients by solving the SA-CPMCSCF equations forced us to reduce the active space to eight electrons in six orbitals. In the trajectories started on S_2 and those running on the n,π^* state (S_1), the active space consisted of the five π orbitals approximately localized on the $N_1-C_6-C_5-C_4-O_8$ fragment and the in-plane O_8 oxygen lone pair. This active space remained stable during those trajectories, and no discontinuities were observed. In the S_1 trajectories on the π,π^* state, the occupation of the oxygen lone pair active orbital was 2.0. This orbital was replaced by the N_3 π orbital at the beginning of these trajectories, and the corresponding active space also remained stable.

The initial conditions of the dynamics calculations were obtained by sampling the transition state zero-point energy, which generated a random set of $3N - 7$ coordinates with the corresponding kinetic energy distribution.[23,38] To model the approach to a conical intersection and drive the trajectories in that direction, 1 kcal/mol of extra kinetic energy was added to the mode with the imaginary frequency. The trajectories were run with the analytical Hessian for the first few steps, after which a Hessian updating algorithm[39] was used. The updating algorithm failed to conserve the total energy in 11 out of 25 trajectories, which had to be discarded. The remaining 14 trajectories are the ones discussed in the paper. Energy plots for these trajectories are provided in the Supporting Information.

Results

Potential Energy Surface Calculations. The paths sketched in Figure 1 have been characterized with CASSCF/6-311G* minimum-energy-path calculations from the FC structure on the π,π^* state (see Figure 2, which includes the structures of the critical points). Similar to what is described in ref 16, the resulting path depends on the CASSCF active space used in the calculation. The calculation with a (10,8) active space leads directly to $(Eth)_X$.[16] Along the first steps of this path, the molecule stays planar, and the C_5-C_6 and C_4-O_8 bonds are expanded to approximately 1.5 and 1.25 Å, respectively. Later on, the molecule loses its planarity, and the C_4-O_8 bond is contracted again to its initial value. Thus, structure $(Eth)_X$ has a short C_4-O_8 and a long C_5-C_6 bond (1.19 and 1.45 Å, respectively), and the methyl group is twisted out of the plane of the ring. In contrast to this, the calculation with the (12,9) active space leads to a quasi-planar minimum on the π,π^* state, $(\pi,\pi^*)_{Min}$. The main difference with the first path is that the C_4-O_8 bond is expanded to approximately 1.36 Å, and the methyl group stays in the plane of the molecule. From $(\pi,\pi^*)_{Min}$,

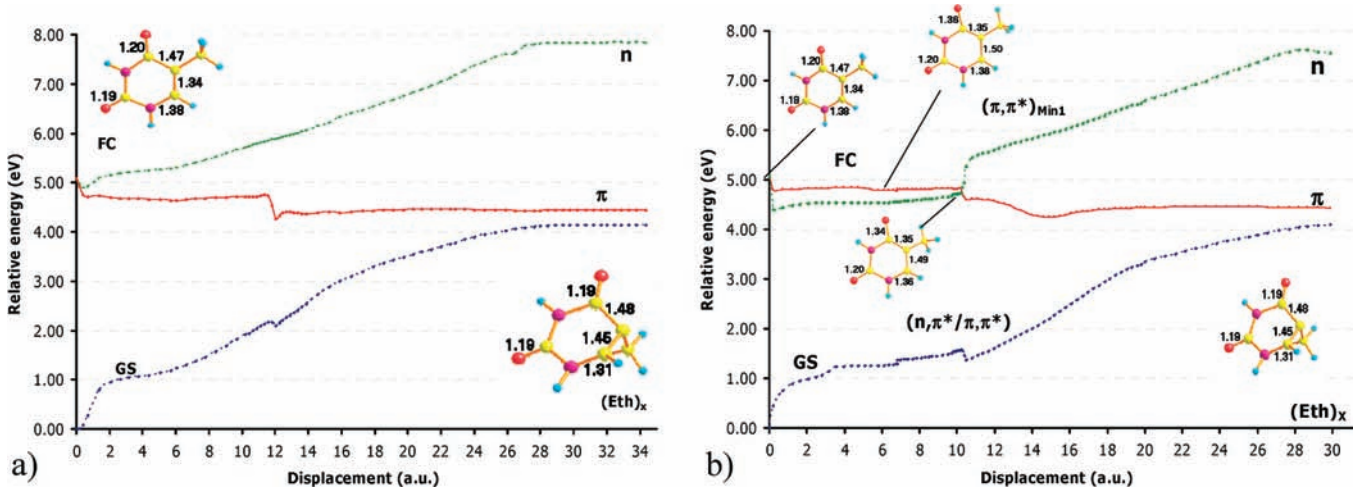

Figure 2. MS-CASPT2(12,9) energy profiles along the CASSCF/6-311G* minimum-energy paths from the FC structure; (a) direct path (path 1 in Figure 1); (b) indirect path (path 2 in Figure 1).

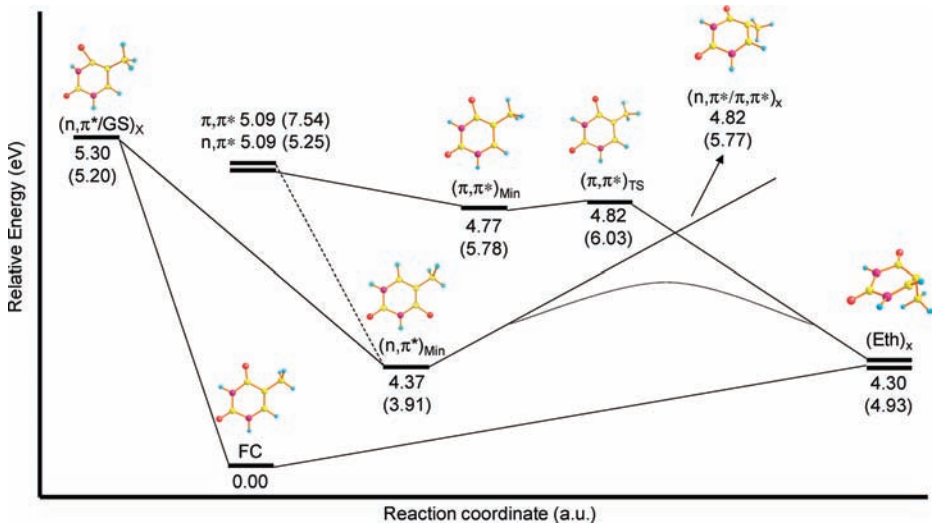

Figure 3. Energies of relevant critical points on the excited-state surface of thymine at the MS-CASPT2(12,9)/6-311G* level of theory (CASSCF(8,6)/6-31G* optimized energies in brackets).

we have characterized an indirect path similar to the one reported in ref 13. This path continues along a transition structure, $(\pi,\pi^*)_{TS}$, and a conical intersection with the n,π^* state, $(\pi,\pi^*/n,\pi^*)_X$, and ends at $(Eth)_X$. To compare the energies of the two paths, the energy profiles have been recalculated at the MS-CASPT2 level, using a (12,9) active space that includes all π orbitals and the oxygen lone pair involved in the n,π^* excitation. The MS-CASPT2(12,9) energy profiles along the direct and indirect paths are shown in Figure 2a and b, respectively. The MS-CASPT2 barriers along the two paths are small (<0.1 eV), and the discontinuities around 10 au in both profiles are due to degeneracies of the CASSCF reference wave function. The two MS-CASPT2 profiles are similar in energy, and from the static calculations, it is not clear which of the two paths is preferred.

The possibility of populating the n,π^* state along the indirect path and the fate of this state have been studied by calculating the decay path from $(\pi,\pi^*/n,\pi^*)_X$ on the n,π^* state, which leads to a minimum, $(n,\pi^*)_{Min}$. This minimum is characterized by a long C_4-O_8 bond (1.37 Å) and C_6 pyramidalization. From this minimum, we have optimized a decay path through a conical intersection with the ground state, $(n,\pi^*/GS)_X$. This intersection is similar to structure MXS4 from ref 19, with the C_4-O_8 bond stretched to 1.44 Å and a distorted ring. The MS-CASPT2 energy is 5.3 eV, which is higher than the vertical excitation of 5.1 eV. In addition to that, the $(n,\pi^*)_{Min}$ population can also decay through $(Eth)_X$ via a switch back to the π,π^* state. This path will involve an avoided crossing near $(\pi,\pi^*/n,\pi^*)_X$, and its estimated barrier is the difference between $(n,\pi^*)_{Min}$ and $(\pi,\pi^*/n,\pi^*)_X$, 0.4 eV.

The MS-CASPT2 static picture is summarized in Figure 3, and the CASSCF(8,6) energies of the critical points (see Computational Details) are shown in brackets for comparison. There are several differences between the MS-CASPT2 and CASSCF energy profiles. The largest dynamic correlation effect is found along the initial part of the indirect path. The vertical π,π^* and n,π^* excitation energies are approximately 5.1 eV at the MS-CASPT2 level. However, the π,π^* excitation energy is increased by more than 2 eV at the CASSCF level, and the CASSCF barrier between $(\pi,\pi^*)_{Min}$ and $(Eth)_X$ is overestimated by 0.2 eV with respect to the MS-CASPT2 value. Another relevant difference regards the energy of $(n,\pi^*/GS)_X$ relative to the vertical excitation. At the CASSCF level, the intersection lies below the vertical excitation and is accessible (see below), but at the MS-CASPT2 level, it lies higher in energy than the FC structure.

Dynamics Simulations. The CASSCF trajectories started at the FC structure in ref 13 follow the indirect path and get trapped at $(\pi,\pi^*)_{Min}$ for at least 500 fs. For this reason, the dynamics

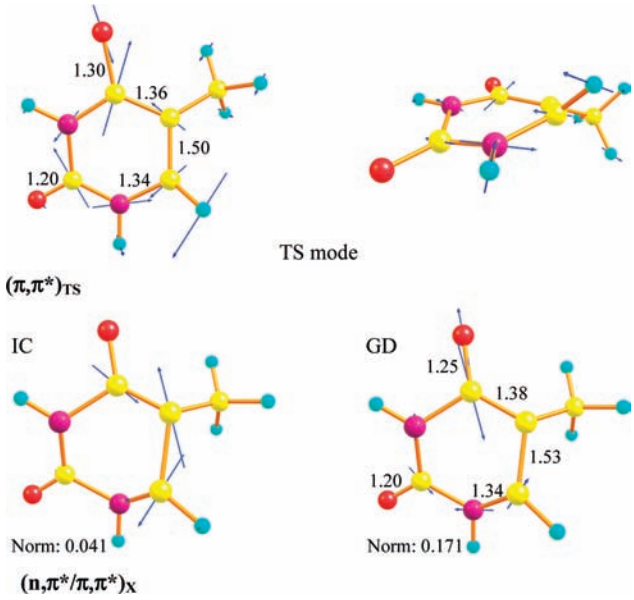

Figure 4. Transition vector at $(\pi,\pi^*)_{TS}$ and branching space vectors (interstate coupling, IC, and gradient difference, GD) at $(n,\pi/\pi,\pi^*)_X$, calculated at the CASSCF(8,6)/6-31G* level. Bond lengths in Å. The changes in the bond lengths of $(n,\pi/\pi,\pi^*)_X$ with respect to Figure 2b are due to the shift of the crossing at the MS-CASPT2 level.

were started at $(\pi,\pi^*)_{TS}$ on S_2, following the transition vector direction toward $(n,\pi^*/\pi,\pi^*)_X$, and $(Eth)_X$. $(\pi,\pi^*)_{TS}$ is characterized by a weak boat-like puckering of the ring and a slightly pyramidalized methyl group ($C_9-C_5-C_4-N_3$ dihedral angle: −153.9°). The most relevant bond distances have a mixed single−double bond character (C_4-O_8: 1.29 Å; C_4-C_5: 1.36 Å; C_5-C_6: 1.49 Å). The transition vector (Figure 4) is mainly composed of C_4-O_8 shortening, C_5-C_6 lengthening, and pyramidalization of N_1 and C_6.

Figure 5 shows the evolution of the three lowest excited states of thymine together with the C_4-O_8 distance along time for a representative trajectory. The state followed by the trajectory is shown with a bold red line. We center on the approach to the CI seam along the reaction coordinate. Thus, the gradient difference vector at the seam (Figure 4) is similar to the transition vector (large C_4-O_8 stretch component), and the seam lies approximately perpendicular to the coordinate (see Figure 1). For this reason, the seam is reached from the TS in a few fs. The trajectory oscillates back and forth around the seam, and the oscillations are approximately in phase with the C_4-O_8 stretching mode (see the evolution of the C_4-O_8 distance in Figure 5). Each oscillation on S_2 is associated with an "adiabatic switch" between the π,π^* and n,π^* states, until the trajectory hops to S_1. In the example shown in Figure 5, the hop to S_1 takes place at the third approach to the seam, and the trajectory continues on the π,π^* state. Once the trajectories decay to the π,π^* state, the C_4-O_8 bond is shortened, while this bond is stretched for those trajectories that decay to the n,π^* state.

After the hop to S_1, all trajectories are continued to monitor their subsequent relaxation on the π,π^* or n,π^* state, reducing the number of roots to two (see Computational Details). Out of 14 valid trajectories (see Computational Details), 9 stay on the π,π^* state after the S_2/S_1 crossing, and 5 populate the n,π^* state. A representative trajectory for the decay of the π,π^* state on S_1 is shown in Figure 6. In this case, the C_4-O_8 bond remains short and oscillates around 1.2 Å, while the C_5-C_6 bond is stretched up to 2 Å. At the same time, the methyl starts to bend out of plane. The C_5-C_6 bending and methyl out-of-plane coordinates are contained in the branching space vectors at $(Eth)_X$ (see Figure 7) and take the trajectory to the S_1/S_0 seam of intersection centered around this structure. The decay to the ground state takes place 15−200 fs after the hop from S_2 to S_1 at geometries where the out-of-plane bending angle of the methyl group ranges from 50 to 100° and the C_2-C_3 bond length ranges from 1.2 to 2.0 Å. After the hop to S_0, the "hot" molecule keeps vibrating in the ground state. In the condensed phase (solution or DNA environment), the vibrational excess energy will be dissipated to the environment.

In contrast to the π,π^* trajectories, the trajectories on the n,π^* state are mainly driven by the C_4-O_8 stretch coordinate. This coordinate takes the molecule to a seam of intersection with the ground state, which is reached in about 10 fs (see Figure 8 for a representative trajectory). At the seam region, the C_4-O_8 distance is larger than 1.5 Å. The trajectories oscillate around the seam, and three out of five trajectories decay to the ground state after 100 fs or less. The remaining two trajectories reach the computational time limit without decaying to S_0, but it can be assumed that they will decay shortly after that. However, the analysis of the intersection and the comparison with the MS-CASPT2 energies show that the propensity for this decay is overestimated in the dynamics (see Figure 3). At the CASSCF level, the energy of the starting point, $(\pi,\pi^*)_{TS}$, is approximately 0.8 eV higher than $(n,\pi^*/GS)_X$, and the intersection is energetically accessible, but at the MS-CASPT2 level, the minimum of the $(n,\pi^*/GS)_X$ seam lies slightly higher in energy than the FC point. The decay through this intersection is therefore less favored at the higher level of theory.

Discussion

The indirect excited-state decay path of thymine shown in Figure 1 has been studied with semiclassical dynamics started at the transition state that separates the minimum from the conical intersection with the ground state, $(Eth)_X$. Qualitatively, our results are similar to those found in a semiempirical OM2/MRCI dynamics study after excitation to the FC region.[17] Thus, the trajectories are funneled along the decay path toward an S_2/S_1 conical intersection seam between the π,π^* and n,π^* states which is perpendicular to the decay coordinate (C_4-O_8 bond stretch; see Figure 1). The quenching to the S_1 state is highly efficient and takes place in 5−60 fs, and a branching of the trajectories between the π,π^* and n,π^* states is observed. The trajectories that stay on the π,π^* state continue to the S_1/S_0 seam associated to $(Eth)_X$ and decay to the ground state in 200 fs or less. The trajectories that decay on the n,π^* state also reach a seam of conical intersection where they decay to the ground state on a similar time scale, but comparison with MS-CASPT2 calculations shows that the CASSCF trajectories overestimate the probability of this decay.

Experimentally, the short-time excited-state photodynamics of thymine are described with one or two components in the femtosecond range and one component in the picosecond range. From the present CASSCF dynamics and the previous study of the decay from the FC structure, this multiexponential decay could be associated with the indirect path shown in Figure 1, as already proposed.[13] In this case, the first step of the decay would correspond to the decay to $(\pi,\pi^*)_{Min}$ on the fs scale, and the second step would correspond to the access to $(Eth)_X$ through $(\pi,\pi^*)_{TS}$ on the ps scale. However, comparison of the CASSCF decay paths with the MS-CASPT2 ones shows that this conclusion is not as straightforward as it may seem. At the higher level of theory, there is a direct path (see Figure 1) that could also account for the fs decay component. This path could

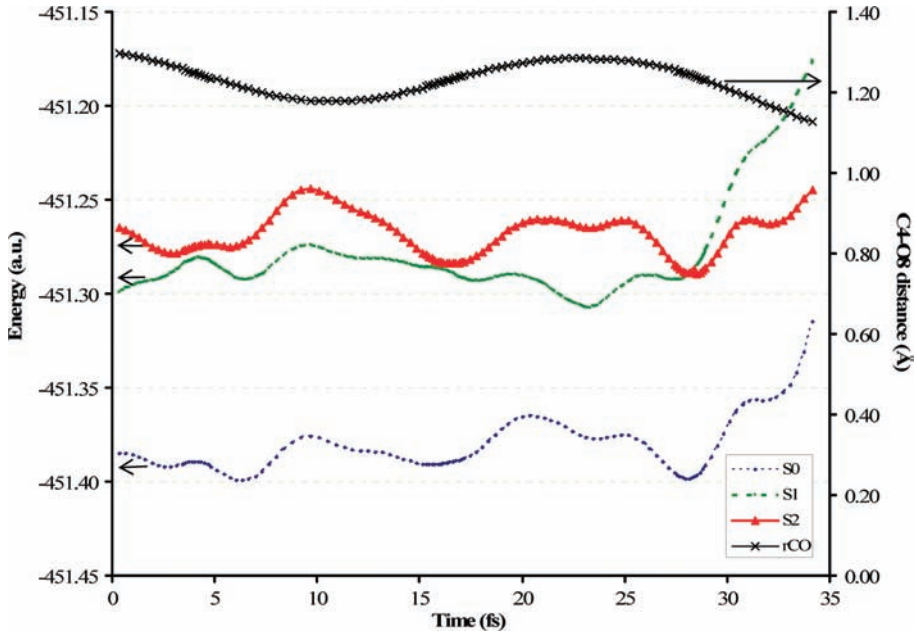

Figure 5. Time evolution of the CASSCF(8,6) energy of the S_0-S_2 states of thymine and the C_4-O_8 distance for a representative trajectory on S_2 from $(\pi,\pi^*)_{TS}$. The label of the states refers to the order at the beginning of the trajectory.

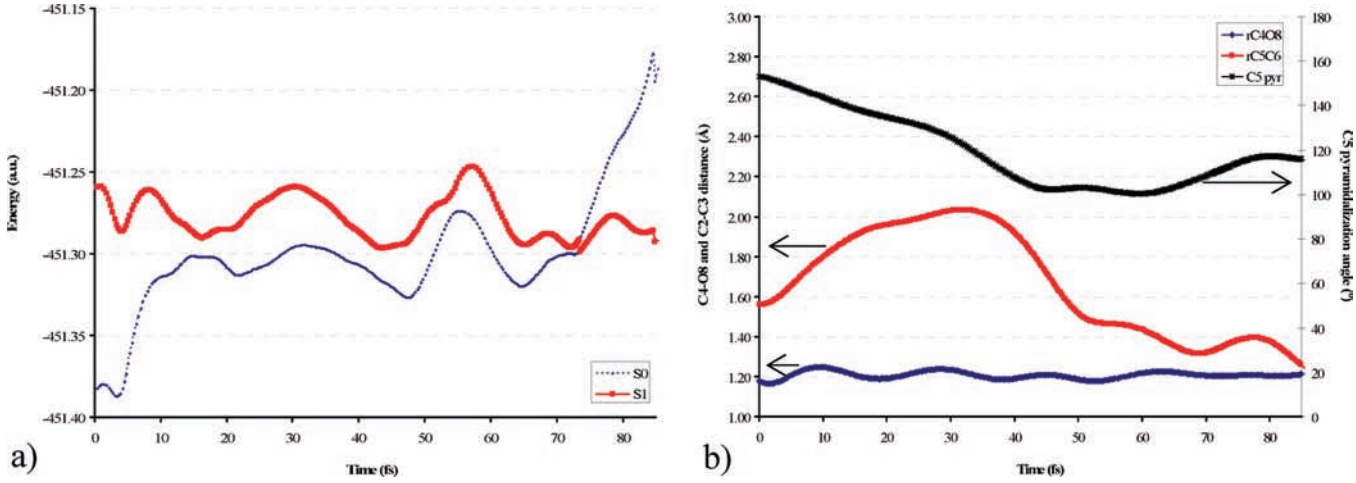

Figure 6. (a) Time evolution of the CASSCF(8,6) energy of the S_0-S_1 states of thymine for a representative trajectory on S_1 (π,π^* state); (b) the same for the C_4-O_8 and C_5-C_6 distance and the C_5 pyramidalization ($C_9-C_5-C_4-N_3$ dihedral angle). The labels of the states in (a) refer to the order at the beginning of the trajectory.

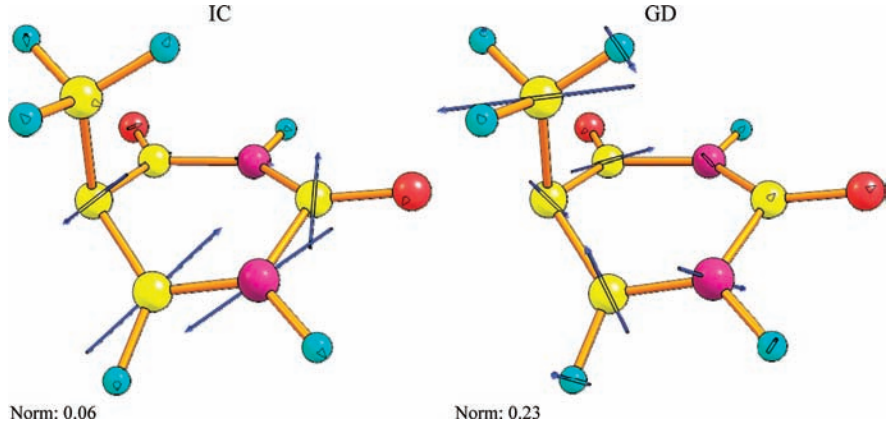

Figure 7. Branching space vectors (interstate coupling, IC, and gradient difference, GD) at $\mathbf{(Eth)_X}$, calculated at the CASSCF(8,6)/6-31G* level.

not be optimized at the CASSCF(8,6)/6-31G* level and is not observed in the short-time dynamics. However, the MS-CASPT2 results show that the direct and indirect paths are very similar from the energetic point of view. It is therefore likely that the CASSCF semiclassical dynamics only explain one side of the story (the indirect decay), while, in reality, the wavepackets

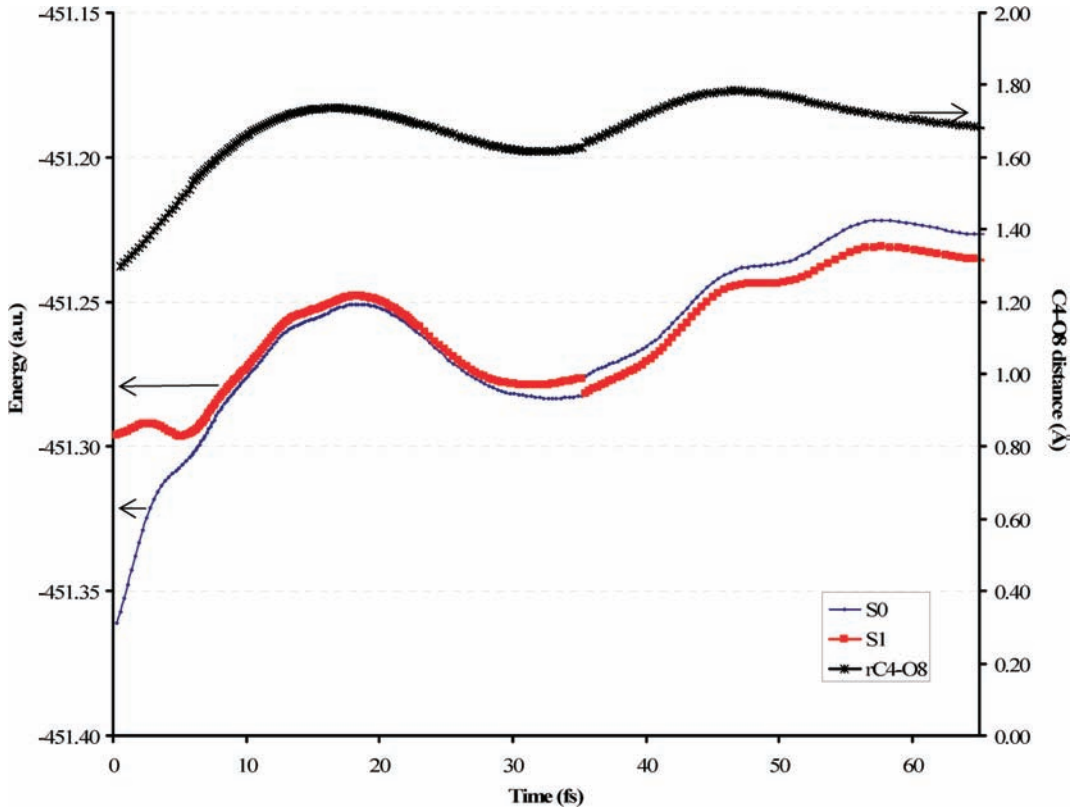

Figure 8. Time evolution of the CASSCF(8,6) energy of the S_0-S_1 states of thymine and the C_4-O_8 distance for a representative trajectory on S_1 (n,π^* state). The label of the states refers to the order at the beginning of the trajectory.

created by the excitation may be distributed along the two paths shown in Figure 1. The MS-CASPT2 energy profile along the indirect path also suggests that the lifetime of $(\boldsymbol{\pi,\pi^*})_{\mathbf{Min}}$ is overestimated by the CASSCF trajectories as the barrier that separates it from $(\mathbf{Eth})_{\mathbf{X}}$ is substantially lowered at the dynamically correlated level. Thus, the estimated MS-CASPT2 value is approximately 0.1 eV (800 cm^{-1}). In this case, the lifetime of $(\boldsymbol{\pi,\pi^*})_{\mathbf{Min}}$ will mainly depend on intrastate vibrational redistribution from the in-plane modes activated in the first part of the decay to the TS mode, and this process can be expected to be quite efficient as the TS mode also has a large in-plane component (see Figure 4). Therefore, it is likely that the lifetime of $(\boldsymbol{\pi,\pi^*})_{\mathbf{Min}}$ lies in the subpicosecond range. This suggests that the experimental subpicosecond decay component(s) reflects the quenching to the ground state along both direct and indirect paths.

Comparison between the CASSCF and MS-CASPT2 energies is also necessary to discuss the lifetime of the n,π^* state in the dynamics. The CASSCF trajectories on the n,π^* state decay to the ground state quickly because the energy of the $(\mathbf{n,\pi^*/GS})_{\mathbf{X}}$ intersection seam is below the energy of $(\boldsymbol{\pi,\pi^*})_{\mathbf{TS}}$, the dynamics starting point. This is similar to the OM2/MRCI dynamics study, where the lifetime of the n,π^* state is less than 1 ps because the minimum-energy intersection between the n,π^* and the ground state lies 1 eV below the FC point.[17] However our relative MS-CASPT2 energies show that the short n,π^* lifetime may be an artifact of the CASSCF and OM2 methods. Thus, the relative MS-CASPT2 energy of the $(\mathbf{n,\pi^*/GS})_{\mathbf{X}}$ intersection minimum, which marks the threshold for decay of the n,π^* state along this route, is 5.3 eV. This value is above the calculated vertical excitation of approximately 5.1 eV (see Figure 3). Other intersection minima of $(\mathbf{n,\pi^*/GS})$ character, such as the intersection labeled MXS3 in ref 19, lie higher in energy at the MS-CASPT2 level. This suggests that the decay of the n,π^* state along this route will only take place at excitation wavelengths of 230−240 nm or less. At lower excitation energies, there are other decay paths available for $(\boldsymbol{n,\pi^*})_{\mathbf{Min}}$. The first one is the decay through $(\mathbf{Eth})_{\mathbf{X}}$. This path goes through an avoided crossing between the π,π^* and n,π^* states associated to a MS-CASPT2 barrier of approximately 0.4 eV (see Figure 3) and is not observed in the dynamics because the trajectories are biased toward the $(\mathbf{n,\pi^*/GS})_{\mathbf{X}}$ intersection. The second path is intersystem crossing to the triplet state. This process is possible due to the large spin−orbit coupling[40] of approximately 60 cm^{-1}, but it has been not observed in our dynamics because only singlet states are considered. However, the presence of these two paths suggests that the decay component of approximately 5 ps determined experimentally may correspond to the lifetime of the n,π^* state.

Conclusions

The excited-state decay of the lowest π,π^* state of thymine has been studied with MS-CASPT2 static calculations and CASSCF semiclassical on-the-fly dynamics. The MS-CASPT2 calculations are used to complete the picture of the dynamics, which suffers from the limitations of the CASSCF method. Our conclusions can be summarized with the help of Figure 1. Two paths, a direct one and an indirect one, lead from the FC structure to $(\mathbf{Eth})_{\mathbf{X}}$, a conical intersection with the ground state. At the MS-CASPT2 level, using a CASSCF(12,9) reference wave function, both paths have similar slopes. This suggests that both paths will be initially populated after the excitation pulse. The indirect path goes through a shallow minimum of the π,π^* state, $(\boldsymbol{\pi,\pi^*})_{\mathbf{Min}}$. Its lifetime can be assumed to lie in the subpicosecond range in view of the small barriers and taking into account that the experiments are carried out at high temperatures (400−500 K). After the barrier, the CASSCF

dynamics from $(\pi,\pi^*)_{TS}$ show that some of the trajectories quickly evolve to $(Eth)_X$, where they are quenched efficiently to the ground state. The trajectories that reach $(Eth)_X$ along the direct path will be quenched with a similar efficiency. Therefore, we propose that the experimental subpicosecond decay component(s) come from the two groups of trajectories (direct decay and indirect decay staying on the π,π^* state). In addition to that, we assign the picosecond component to the n,π^* state populated along the indirect path. Other aspects of the photodynamics, like the relative importance of the direct and indirect paths, remain unresolved and will require an improvement of the dynamics approach for a more accurate simulation.

Acknowledgment. We thank L. González (Univ. Jena, Germany) and T. Schultz (Max-Born-Institut Berlin, Germany) for helpful discussions. This work has been supported by Grants CTQ2005-04563 and CTQ2008-06696 from the Spanish Ministerio de Ciencia e Innovación (MICINN) and grant EP/F028296/1 from EPSRC UK. D. Asturiol acknowledges a MICINN Ph. D. grant (FPU Grant No. AP2004-4774).

Supporting Information Available: Complete refs 27, 31, and 36. Absolute energies of stationary points, CASSCF(8,6)/6-31G* energy profile for the linear interpolation in internal coordinates along the indirect path, energy plots for the 14 valid trajectories, and Cartesian coordinates of structures. This material is available free of charge via the Internet at http://pubs.acs.org.

Note Added in Proof. A paper describing photodynamics simulations of the S_2/S_1 decay of thymine has appeared after submission of our manuscript (Szymczak, J. J.; Barbatti, M.; Soo Hoo J. T.; Adkins, J. A.; Windus, T. L.; Nachtigallová, D.; Lischka, H. *J. Phys. Chem. A* **2009**, *113*, in press. doi: 10.1021/jp905085x).

References and Notes

(1) Canuel, C.; Mons, M.; Piuzzi, F.; Tardivel, B.; Dimicoli, I.; Elhanine, M. *J. Chem. Phys.* **2005**, *122*, 074316.

(2) Crespo-Hernandez, C. E.; Cohen, B.; Hare, P. M.; Kohler, B. *Chem. Rev.* **2004**, *104*, 1977–2019.

(3) Kang, H.; Lee, K. T.; Jung, B.; Ko, Y. J.; Kim, S. K. *J. Am. Chem. Soc.* **2002**, *124*, 12958–12959.

(4) Pecourt, J. M. L.; Peon, J.; Kohler, B. *J. Am. Chem. Soc.* **2001**, *123*, 10370–10378.

(5) Pecourt, J. M. L.; Peon, J.; Kohler, B. *J. Am. Chem. Soc.* **2001**, *123*, 5166–5166.

(6) Peon, J.; Zewail, A. H. *Chem. Phys. Lett.* **2001**, *348*, 255–262.

(7) Ullrich, S.; Schultz, T.; Zgierski, M. Z.; Stolow, A. *Phys. Chem. Chem. Phys.* **2004**, *6*, 2796–2801.

(8) He, Y. G.; Wu, C. Y.; Kong, W. *J. Phys. Chem. A* **2003**, *107*, 5145–5148.

(9) He, Y. G.; Wu, C. Y.; Kong, W. *J. Phys. Chem. A* **2004**, *108*, 943–949.

(10) Cadet, J.; Vigny, P.; Morrison, H. The Photochemistry of Nucleic Acids. In *Bioorganic Photochemistry*; John Wiley & Sons Inc.: New York, 1990; Vol. 1.

(11) Shukla, M.; Leszczynski, J. *Radiation Induced Molecular Phenomena in Nucleic Acids: A Comprehensive Theoretical and Experimental Analysis*; Springer: New York, 2008; Vol. 5.

(12) Kang, H.; Lee, K. T.; Kim, S. K. *Chem. Phys. Lett.* **2002**, *359*, 213–219.

(13) Hudock, H. R.; Levine, B. G.; Thompson, A. L.; Satzger, H.; Townsend, D.; Gador, N.; Ullrich, S.; Stolow, A.; Martinez, T. J. *J. Phys. Chem. A* **2007**, *111*, 8500–8508.

(14) Lan, Z.; Fabiano, E.; Thiel, W. *J. Phys. Chem. B* **2009**, *113*, 3548–3555.

(15) Matsika, S. *J. Phys. Chem. A* **2004**, *108*, 7584–7590.

(16) Merchan, M.; Gonzalez-Luque, R.; Climent, T.; Serrano-Andres, L.; Rodriuguez, E.; Reguero, M.; Pelaez, D. *J. Phys. Chem. B* **2006**, *110*, 26471–26476.

(17) Mercier, Y.; Santoro, F.; Reguero, M.; Improta, R. *J. Phys. Chem. B* **2008**, *112*, 10769–10772.

(18) Perun, S.; Sobolewski, A. L.; Domcke, W. *J. Phys. Chem. A* **2006**, *110*, 13238–13244.

(19) Zechmann, G.; Barbatti, M. *J. Phys. Chem. A* **2008**, *112*, 8273–8279.

(20) Zgierski, M. Z.; Patchkovskii, S.; Fujiwara, T.; Lim, E. C. *J. Phys. Chem. A* **2005**, *109*, 9384–9387.

(21) Nieber, H.; Doltsinis, N. *Chem. Phys.* **2008**, *347*, 405–412.

(22) Paterson, M. J.; Hunt, P.; Robb, M. A.; Takahashi, O. *J. Phys. Chem. A* **2002**, *106*, 10494–10504.

(23) Worth, G. A.; Hunt, P.; Robb, M. A. *J. Phys. Chem. A* **2003**, *107*, 621–631.

(24) Weingart, O.; Migani, A.; Olivucci, M.; Robb, M. A.; Buss, V.; Hunt, P. *J. Phys. Chem. A* **2004**, *108*, 4685–4693.

(25) Hunt, P. A.; Robb, M. A. *J. Am. Chem. Soc.* **2005**, *127*, 5720–5726.

(26) Barbatti, M.; Lischka, H. *J. Am. Chem. Soc.* **2008**, *130*, 6831–6839.

(27) Frisch, M. J.; et al. *Gaussian 03*, revision C.01; Gaussian, Inc.: Pittsburgh, PA, 2003.

(28) Gonzalez, C.; Schlegel, H. B. *J. Chem. Phys.* **1989**, *90*, 2154–2161.

(29) Celani, P.; Robb, M. A.; Garavelli, M.; Bernardi, F.; Olivucci, M. *Chem. Phys. Lett.* **1995**, *243*, 1–8.

(30) Yamamoto, N.; Vreven, T.; Robb, M. A.; Frisch, M. J.; Schlegel, H. B. *Chem. Phys. Lett.* **1996**, *250*, 373–378.

(31) Karlstrom, G.; et al. *Comput. Mater. Sci.* **2003**, *28*, 222–239.

(32) Lorentzon, J.; Fulscher, M. P.; Roos, B. O. *J. Am. Chem. Soc.* **1995**, *117*, 9265–9273.

(33) Chen, W. *Chem. Phys. Lett.* **1994**, *228*, 436–442.

(34) Helgaker, T. *Chem. Phys. Lett.* **1990**, *173*, 145–150.

(35) Warshel, A. *Chem. Phys. Lett.* **1975**, *32*, 11–17.

(36) Frisch, M. J.; et al. *Gaussian 03*, revision B.07 (Developement version); Gaussian, Inc.: Pittsburgh, PA, 2003.

(37) Blancafort, L.; Hunt, P.; Robb, M. A. *J. Am. Chem. Soc.* **2005**, *127*, 3391–3399.

(38) Tannor, D. *J. Chem. Phys.* **1986**, *85*, 5805–5820.

(39) Bofill, J. M. *J. Comput. Chem.* **1994**, *15*, 1–11.

(40) Serrano-Perez, J. J.; Gonzalez-Luque, R.; Merchan, M.; Serrano-Andres, L. *J. Phys. Chem. B* **2007**, *111*, 11880–11883.

JP905303G